Torque Ripple Reduction in BLDC Torque Motor With Nonideal Back EMF

Jiancheng Fang, Haitao Li, and Bangcheng Han

***Abstract*—In order to improve the speed precision and stabilization of the gimbal servo system of double gimbal magnetically suspended control moment gyro, a comprehensive analysis of the reason of electromagnetic torque ripples of brushless direct current motor with nonideal back electromotive force (EMF) drives in the conduction and commutation regions is presented. A novel automatic control method of torque is proposed. With this method, the current control rule is designed, and the duty cycle of pulse width modulation (PWM) is regulated in real time by measuring the wave function of back EMF. In order to eliminate the diode freewheeling of the inactive phase, the PWM_ON_PWM scheme is used. Simulation and experiment results are given to show that, compared with the conventional current control method, the proposed method can reduce the torque ripple effectively and improve the speed precision and stabilization as well.**

***Index Terms*—Automatic control of torque, brushless direct current (BLDC) motors, double gimbal magnetically suspended control moment gyro (DGMSCMG), electromagnetic torque ripple, nonideal back electromotive force (EMF).**

I. Introduction

CONTROL moment gyro (CMG) is considered to be one of the primary actuators used for the attitude control of large spacecrafts [1]. The actuator with high-precision, fast-response, and large-angle maneuver characteristics is necessary for the attitude control of spacecraft. Magnetically suspended control moment gyro (MSCMG) has the advantage of high precision and longevity owing to the zero friction and enhanced damping of high-speed rotor [2]. The gimbal servo system is an important part of MSCMG and its control precision of angular position and angular speed has a severe influence on the properties of the moment output [3]. Brushless direct current (BLDC) motors have characteristics of high reliability, simple frame, and small friction. By comparing with PMSM, BLDC motor has the advantages of high speed adjusting performance and power density [4], [5]. So, the BLDC motor is the ideal choice for the CMG's gimbal system. Therefore, its application in the high-precision servo system is restricted due to the electromagnetic torque ripple [6].

The torque ripple reduction and the control performance improvement of BLDC have been the research hotspot in recent years, and the main research works are focused on commutation torque ripple, the torque ripple produced by diode freewheeling of inactive phase, and the torque ripple caused by the nonideal back electromotive force (EMF). For the commutation torque ripple, Calson *et al*. proposed that relative torque is related to current and varies with speed [7]. In [6], a single dc current sensor and an adaptive phase-change point regulation scheme should be used to suppress the commutation torque ripple, but the diode freewheeling of inactive phase was not considered. Chuang *et al*. have analyzed the influences of different pulse width modulation (PWM) patterns on the commutation torque ripples according to the BLDC motors with ideal trapezoidal back EMF [8], and indicated that the PWM_ON pattern is better. In [9], in order to suppress the commutation torque ripple of the BLDC motors with unbalanced hall sensors, speed filter is used to regulate the phase-change point automatically. However, this control method is more competent under the high-speed working condition. In [10], the reasons of commutation torque ripple for low and high speeds are analyzed. In order to keep incoming and outgoing phase currents changing at the same rate during commutation, the duty cycle was regulated at low speed and the deadbeat current control was adopted at high speed, but the nonideal back EMF was not considered in this method. It is an effective way to propose some topology circuit for BLDC motor drives to control their dc-link voltage, as shown by some researchers presented in [11]–[13]. In reference [11], a buck converter is used to regulate dc-link voltage to reduce the commutation torque ripple, but the bandwidth of buck converter was not considered, so this structure can only satisfy torque pulsation at low speed. Chen *et al*. propose a superlift Luo topology circuit to produce desired dc-link voltage [12], but this structure is more complex and competent only under high-speed condition. In [13], a SEPIC topology circuit is employed, but this topology structure needs to add three switches and their corresponding inductances, capacitances, and diodes.

For the diode freewheeling of inactive phase, various modulation methods have been analyzed, the PWM_ON_PWM and PWM_PWM methods are considered, which can eliminate the diode freewheeling of inactive phase. Considering the power dissipation, PWM_ON_PWM is the better modulation method [14], [15].

In view of the torque ripples of BLDC motor with nonideal back EMF, there are mainly two kinds of resolvents. One is to employ direct torque control to regulate current [16]–[19], and the other is to apply the motor's back EMF waveform functions to regulate the current [20]–[23]. In [16], the direct torque control method is adopted, but the back EMF and phase current need to be measured. So, the complexity of the circuit and software is increased. In [18], DSC control method is introduced into the BLDC motor, but the characteristic of nonideal back

Manuscript received May 27, 2011; revised August 24, 2011 and October 9, 2011; accepted October 29, 2011. Date of current version June 20, 2012. Recommended for publication by Associate Editor G. Oriti.

The authors are with the School of Instrument Science and Optoelectronics Engineering, Beijing University of Aeronautics and Astronautics, Beijing 100083, China (e-mail: fangjiancheng@buaa.edu.cn; greatlht@163.com; hanbangcheng@buaa.edu.cn).

Color versions of one or more of the figures in this paper are available online at http://ieeexplore.ieee.org.

Digital Object Identifier 10.1109/TPEL.2011.2176143

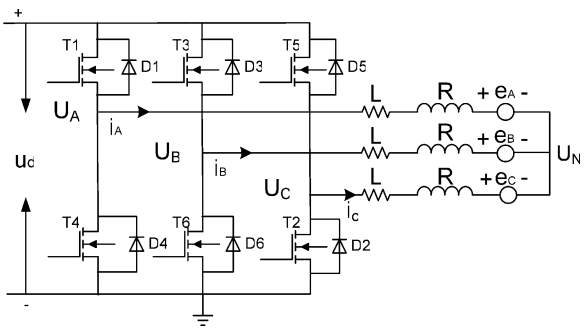

Fig. 1. Block diagram of BLDCM drive system.

EMF was not considered. In [19], a predictive control method was used to obtain reduced switching frequency while keeping torque within the desired hysteresis band. In [20], the influence of high harmonics on the motor's torque was analyzed. In [21], the control method in which the torque ripple can be reduced by changing the dc-link voltage is analyzed and simulated, but the corresponding topology structure was not given. Aghili *et al*. propose an optimal commutation scheme based on Fourier decomposition with back EMF and estimating the Fourier coefficients to reduce the torque ripple and speed ripple [22], [23]. Lu *et al*. propose a torque method for minimizing the torque ripple of BLDC motor with nonideal back EMF [24], but the diode freewheeling of the inactive phase was not considered and the modulation scheme is PWM_PWM. For space application, the magnets and the sensors of the BLDC motor are made to tight tolerances, so the manufacturing imprecision is not an issue.

This paper proposes a new current control method for the BLDC motors with nonideal back EMF. In this method, PWM_ON_PWM method is used to eliminate the current through the free-wheeling diode when the phase is inactive. The motor's phase current, angular position, and speed are measured in real time and the duty cycle is precalculated in the designed current controller to control the phase current. In addition, commutation time is calculated in the controller. Simulation and experimental results showed that, compared with the conventional current control method, the new current control method can reduce the torque ripple effectively.

II. Design of Torque Control Method

The BLDC motor is considered as three-phase star connected and is fed by a conventional three-phase voltage source inverter. Its configuration is shown in Fig. 1, where R, L, e, U, i, U_N, and U_d represent the armature resistance, inductance, back EMF, terminal voltage, phase current, motor neutral voltage, and dc-link voltage, respectively.

The assumptions made for the development of BLDC motor model are: 1) iron and stray losses are neglected; and 2) three-phase windings are symmetrical. The voltage equations of three windings with phase variables are

$$U_A = Ri_A + L\frac{di_A}{dt} + e_A + U_N \tag{1}$$

$$U_B = Ri_B + L\frac{di_B}{dt} + e_B + U_N \tag{2}$$

$$U_C = Ri_C + L\frac{di_C}{dt} + e_C + U_N. \tag{3}$$

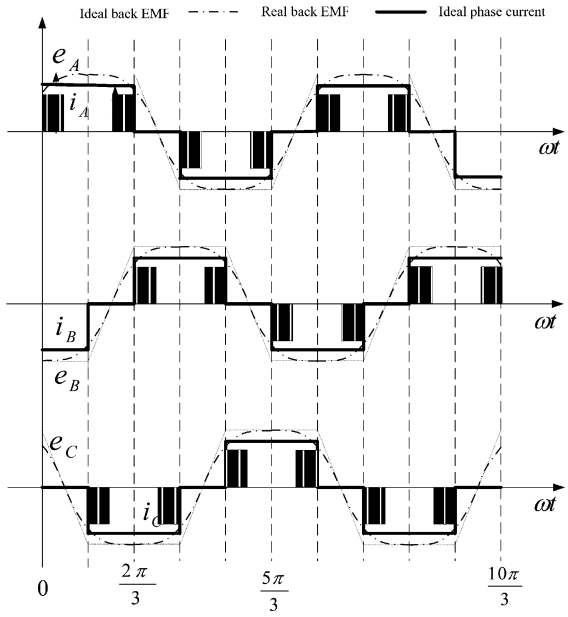

Fig. 2. PWM_ON_PWM pattern.

And the equation of the electromagnetic torque is

$$T_e = \frac{e_A i_A + e_B i_B + e_C i_C}{\omega} \tag{4}$$

where T_e is the electromagnetic torque of motor, ω is the mechanical angular velocity of rotor. As three windings are connected as star, the relationship of three-phase current is

$$i_A + i_B + i_C = 0. \tag{5}$$

A. Normal Conduction Period

In the normal conduction region, two phases are conducted with the selected rotor position, the other phase is inactive and has no current and no contribution to the electromagnetic torque. But when the diode of the MOSFET connected with the inactive phase windings is in ON state once the terminal voltage of the inactive phase is over the dc-link voltage or under the zero voltage, thus, a ripple current flows in the inactive phase during the diode freewheeling and produces the torque ripple. In [14] and [15], a novel PWM mode named PWM_ON_PWM is proposed, which can entirely eliminate the emerging current in the turn-OFF phase during noncommutation period and, thus, reduce the torque ripple during noncommutation period. Its modulation pattern is shown as Fig. 2.

In the $\pi/3 \sim \pi/2$ period, T1 is switched ON and T2 is chopping, the current flows into phase A and then out from phase C, $i_A = -i_C$, $i_B = 0$. According to (4), the torque function can be obtained as

$$T_{e1} = \frac{e_A i_A + e_C i_C}{\omega}. \tag{6}$$

Assuming the duty cycle of switch T2 is D, the phase voltage equations in the normal conduction period can be described as

$$U_A = Ri_A + Ldi_A/dt + e_A + U_N = u_d \tag{7}$$

$$U_B = e_B + U_N \tag{8}$$

$$U_C = Ri_C + Ldi_C/dt + e_C + U_N = (1-D)u_d. \tag{9}$$

So, the neutral voltage can be given as

$$U_N = \frac{2u_d - D \times u_d - e_A - e_C}{2}. \tag{10}$$

Substituting (10) into (7) and (9), respectively, the current derivative functions of phase A and C are shown as follows:

$$\frac{di_A}{dt} = \frac{D \times u_d + e_C - e_A}{2L} \tag{11}$$

$$\frac{di_C}{dt} = \frac{e_A - e_C - D \times u_d}{2L}. \tag{12}$$

As the carrier cycle of PWM is much less than the electrical time constant of stator windings, the effect of motor armature resistance is neglected. Since the sampling time T_s is very short, it is assumed that the phase EMF e_A, e_B, and e_C maintain constant in the sampling time, and the current of phase A and C can be described as

$$i_A(k+1) = \frac{D(k) \times u_d + e_C(k) - e_A(k)}{2L} T_s + i_A(k) \tag{13}$$

$$i_C(k+1) = \frac{e_A(k) - e_C(k) - D(k) \times u_d}{2L} T_s + i_C(k). \tag{14}$$

By combining (13), (14), and (6), the discrete expression of torque in the normal conduction period can be obtained as

$$T(k+1) = T(k) + \frac{D(k)u_d(e_A(k) - e_C(k)) - (e_A(k) - e_C(k))^2}{2L\omega(k)} T_s \tag{15}$$

where $T(k+1)$ is the reference torque T_{ref} of the next period. From (15), the duty cycle $D(k)$, which is the control value of the next period, can be solved as

$$D(k) = \frac{2L\omega(k)(T_{\text{ref}} - T(k)) + (e_A(k) - e_C(k))^2}{u_d(e_A(k) - e_C(k))T_s}. \tag{16}$$

In the $\pi/2 \sim 2\pi/3$ period, switch T2 is ON and T1 is chopping, the current also flows into phase A and out phase C, where $i_A = -i_C, i_B = 0$. The three-phase voltage functions are shown as follows:

$$U_A = Ri_A + Ldi_A/dt + e_A + U_N = D \times u_d \tag{17}$$

$$U_B = e_B + U_N \tag{18}$$

$$U_C = Ri_C + Ldi_C/dt + e_C + U_N = 0. \tag{19}$$

The neutral voltage function and the current derivative functions of phase A and C are shown as

$$U_N = \frac{D \times u_d - e_A - e_C}{2} \tag{20}$$

$$\frac{di_A}{dt} = \frac{D \times u_d + e_C - e_A}{2L} \tag{21}$$

$$\frac{di_C}{dt} = \frac{e_A - e_C - D \times u_d}{2L}. \tag{22}$$

By comparing (21) with (11) and comparing (22) with (12), the duty cycle of the system are same in $\pi/3 \sim \pi/2$ period and $\pi/2 \sim 2\pi/3$ period.

B. Commutation Period

Assuming at a particular commutation process, the current transferring from phase A to phase B is considered, T1 is switched OFF and T2 is switched ON, T3 is chopping, so the three-phases voltage equations are

$$U_A = Ri_A + Ldi_A/dt + e_A + U_N = 0 \tag{23}$$

$$U_B = Ri_B + Ldi_B/dt + e_B + U_N = D \times u_d \tag{24}$$

$$U_C = Ri_C + Ldi_C/dt + e_C + U_N = 0. \tag{25}$$

From the previous three equations, the neutral voltage can be described as

$$U_N = \frac{D \times u_d - e_A - e_B - e_C}{3}. \tag{26}$$

Substituting (26) into (23), (24), and (25), the differential functions of phase current are shown as

$$Ri_A + L\frac{di_A}{dt} = -e_A - U_N = \frac{e_B + e_C - 2e_A - D \times u_d}{3} = u_{a1} \tag{27}$$

$$Ri_B + L\frac{di_B}{dt} = D \times u_d - e_B - U_N = \frac{2D \times u_d + e_A + e_C - 2e_B}{3} = u_{b1} \tag{28}$$

$$Ri_C + L\frac{di_C}{dt} = -e_C - U_N = \frac{e_A + e_B - 2e_C - D \times u_d}{3} = u_{c1}. \tag{29}$$

With the initial conditions of $i_A(t=0) = I$, $i_B(t=0) = 0$, and $i_C(t=0) = -I$, (27) and (28) can be solved as

$$i_A = \frac{u_{a1}}{R} + \left(I - \frac{u_{a1}}{R}\right) e^{-(R/L)t} \tag{30}$$

$$i_B = \frac{u_{b1}}{R} - \frac{u_{b1}}{R} e^{-(R/L)t}. \tag{31}$$

Expanding $e^{-(R/L)t}$ through Taylor series, and neglecting its quadratic term or more. The first-degree term can be derived as

$e^{-(R/L)t} = 1 - (R/L)t$. Substituting it into (30) and (31), the time t_{a1} when i_A decreases from 1 to 0 and the time t_{b1} when i_B increases from 0 to 1 can be solved as

$$t_{a1} = \frac{3IL}{3IR + 2e_A - e_B - e_C + D \times u_d} \tag{32}$$

$$t_{b1} = \frac{3IL}{2D \times u_d + e_A + e_C - 2e_B}. \tag{33}$$

If the motor has no commutation torque ripple on the condition working at PWM_ON_PWM scheme, t_{a1} must be equal to t_{b1}, and neglecting the influence of the resistance, the duty cycle of commutation period can be determined as

$$D(k) = \frac{e_A(k) + e_B(k) - 2e_C(k)}{u_d}. \tag{34}$$

For $0 < D(k) < 1$, it can be deduced from (34) that the commutation torque ripple cannot be restrained through regulating duty cycle of PWM. In [20], overlapping commutation is proposed to restrain the commutation torque ripple. In this method, the switch T1 is still chopping at the time of Δt after phase-change point, and the three-phase voltage equations are

$$U_A = S \times u_d = Ri_A + Ldi_A/dt + e_A + U_N \tag{35}$$

$$U_B = u_d = Ri_B + Ldi_B/dt + e_B + U_N \tag{36}$$

$$U_C = (1 - S) \times u_d = Ri_C + Ldi_C/dt + e_C + U_N \tag{37}$$

where S is the switching function, and $S = 1$ denotes switching ON and $S = 0$ denotes switching OFF. In every carrier cycle of PWM, S maintains 1 during D_2T_s and 0 during $(1 - D_2)\,T_s$, where D_2 is the carrier cycle of PWM, and the neutral voltage U_N can be solved from (35), (36), and (37) shown as follows:

$$U_N = \frac{2u_d - e_A - e_B - e_C}{3}. \tag{38}$$

Substituting (38) into (35) and (36), the influence of the resistance is neglected, and the differential functions of phase current can be described as

$$L\frac{di_A}{dt} = D_2 \times u_d - e_A - U_N = \frac{(3D_2 - 2)u_d + e_B + e_C - 2e_A}{3} = u_{a2} \tag{39}$$

$$Ri_B + Ldi_B/dt = u_d - e_B - U_N = \frac{u_d + e_A + e_C - 2e_B}{3} = u_{b2}. \tag{40}$$

Similarly the time t_{a2} when i_A decrease from 1 to 0 and the time t_{b2} when i_B increase from 0 to 1 can be solved as (41) and (42) with the same method

$$t_{a2} = \frac{3IL}{2e_A - e_B - e_C + (3D_2 - 2) \times u_d} \tag{41}$$

$$t_{b2} = \frac{3IL}{u_d + e_A + e_C - 2e_B} \tag{42}$$

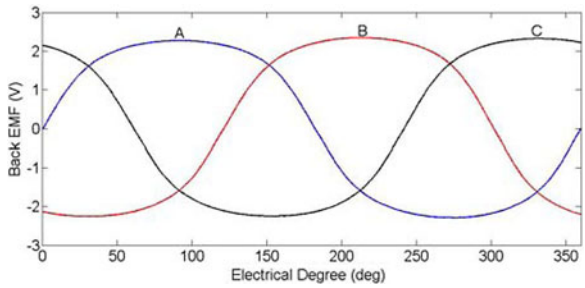

Fig. 3. Measured waveform of back EMF at 5 rad/s.

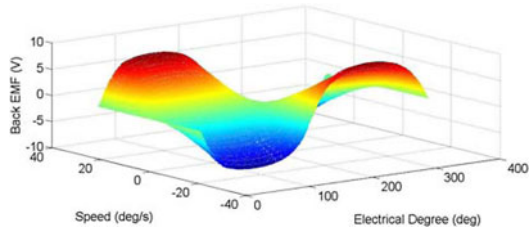

Fig. 4. Measured waveform of angular position, speed, and back EMF.

So the duty cycle of PWM can be solved as (43) when motor works at medium and high speeds

$$D_2(k) = 1 - \frac{e_A(k) + e_B(k) - 2e_C(k)}{3u_d} \tag{43}$$

C. Measuring Method of Back EMF

Because the back EMF of BLDC motor is proportional to the angular speed, the waveform function can be described as

$$\begin{cases} e_A(\theta) = g_A(\theta) \cdot \omega_m \\ e_B(\theta) = g_B(\theta) \cdot \omega_m \\ e_C(\theta) = g_C(\theta) \cdot \omega_m. \end{cases} \tag{44}$$

The angle of motor can be measured from the photoelectric encoder fixed on the motor shaft, so the back EMF of every angle can be measured through offline mode. The waveform of three-phase back EMF is shown as Fig. 3. As the three-phase windings are symmetrical, the difference between two adjacent phases of back EMF is 120° electric angle. So, it is possible to measure the back EMF of phase A only at different speeds, and the corresponding relationship among the motor's angular position, speed, and back EMF are shown as Fig. 4.

III. Simulation Results

To verify the feasibility of the proposed current control algorithm, simulations based on conventional current control algorithm and the new current control algorithm are carried out for the BLDC motor as follows.

The simulated waveforms using H_PWM_L_ON pattern are given in Figs. 5–7. The carrier wave cycle is 20 K and the duty cycle is 50%.

Fig. 5 shows the simulated three-phase current waveform. It shows that the current ripple produced by the nonideal back EMF and changing with commutation exists and there are large

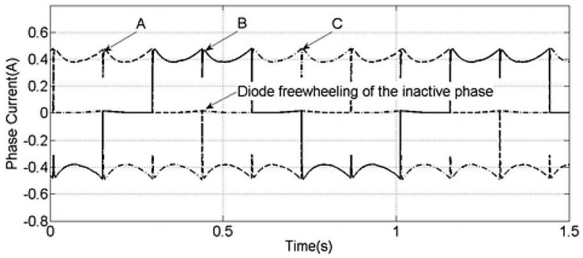

Fig. 5. Simulated currents using H_PWM_L_ON pattern.

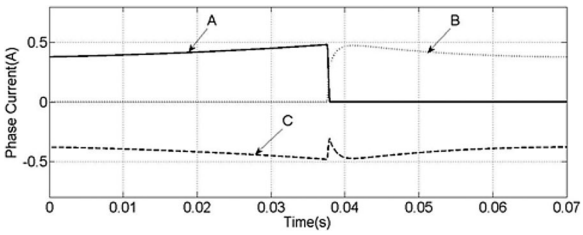

Fig. 6. Phase current using H_PWM_L_ON pattern at commutation period.

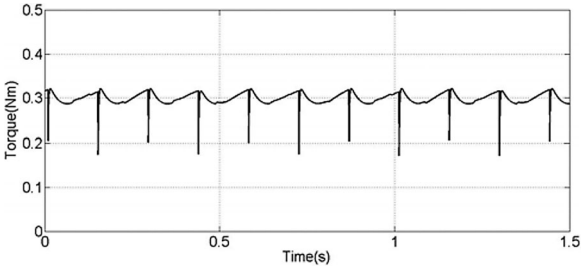

Fig. 7. Simulated torque using H_PWM_L_ON pattern.

current ripples at the phase-change point. Moreover, the current ripples exist on the inactive phase.

Fig. 6 shows three-phase current waveform at the commutation period. During this time, T1 is switched OFF, T3 is switched ON and chopping, and T2 is ON. It shows that the descending rate of phase current A is faster than the rising rate of phase current B, and commutation current ripple is produced on the current of phase C.

Fig. 7 shows the torque waveform using the traditional current control method. In this figure, not only large commutation torque ripple, but also the periodical torque ripple produced by the nonideal back EMF change with current commutation.

The simulated waveforms using a new current controller when motor works at low speed are given in Figs. 8–10. Fig. 8 shows the simulated three-phase current waveform. Comparing with Fig. 5, the commutation torque ripple and the diode freewheeling of the inactive phase are eliminated.

Fig. 9 shows the three-phase current waveform and the PWM waveform of switch T1 and T3 at the commutation period. It can be concluded that, when T1 switches OFF and T3 switches ON, the duty cycle of T3 will be increased, and also the current rising rate of phase B will speed up. So, the current rising rate and the descending rate of phase A are almost equal. There is no ripple on the current of phase C and the commutation torque ripple is eliminated.

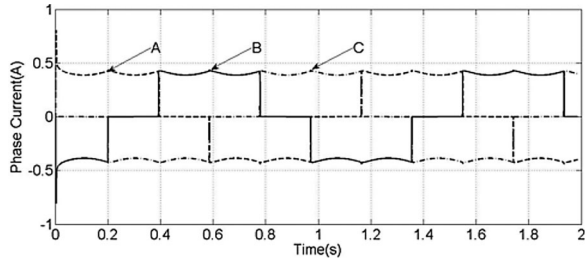

Fig. 8. Simulated current using the new current control method in low speed.

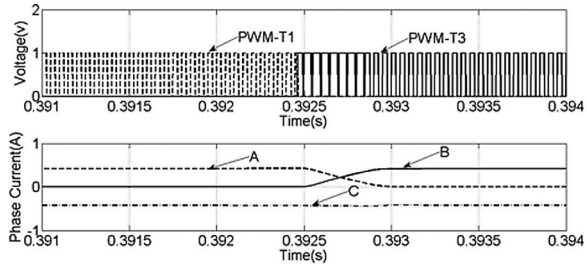

Fig. 9. Simulated current and PWM waveform using the new current control method at commutation period in low speed.

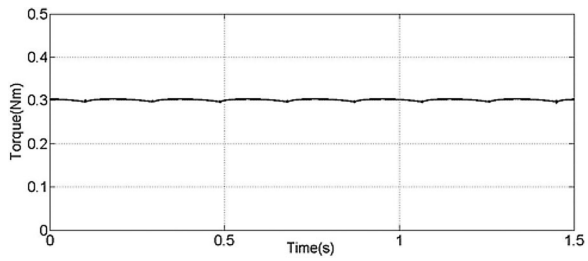

Fig. 10. Simulated torque using the new current control method in low speed.

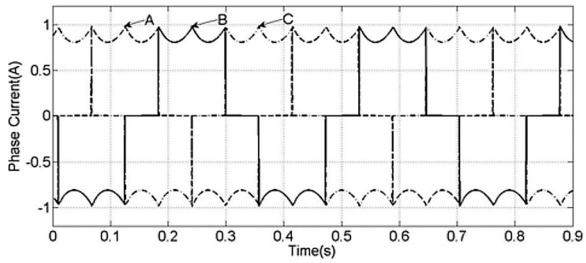

Fig. 11. Simulated current using the new current control method in high speed.

Fig. 10 shows the torque waveform of the motor. Comparing with Fig. 7, the torque ripple is smaller using a new current controller on the condition that the output torque is same.

Figs. 8–10 are given to show the simulated waveforms using a new current controller when motor works at low speed. In Figs. 11 and 12, it can be seen that, when the motor works at high speed and the current transfers from phase A to phase B, the switch of T1 is not OFF and the switch T3 is ON at the phase-change point, and T1 is switched OFF then. With this method, the current rising rate of phase A is equal to the current descending rate of phase B's current, and the commutation torque ripple is restrained. Fig. 13 shows the conclusion. The torque ripple is 6.3% of the outputting torque at high speed using the new current control scheme.

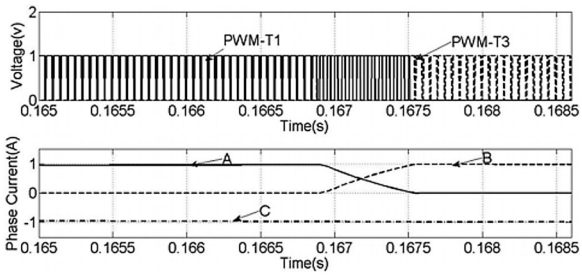

Fig. 12. Simulated current and PWM waveform using the new current control method at commutation period with high speed.

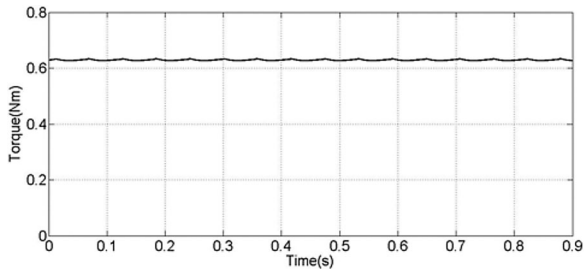

Fig. 13. Simulated torque using the new current control method with high speed.

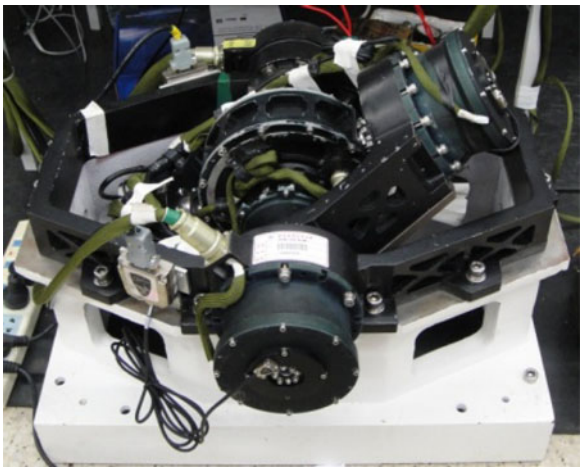

Fig. 14. Experiment system of DGMSCMG.

IV. Experimental Results

In order to validate the feasibility of the new current control method, the 50 N·m·s DGMSCMG is researched and manufactured by the Key Laboratory of Fundamental Science for the National Defense of Novel Inertial Instrument and Navigation System Technology of Beijing University of Aeronautics and Astronautics in 2009. It is used for the experimental research (see Fig. 14) and the experimental parameters are shown in Table I.

The BLDC motor is three-phase star connected and operates in the two-phase conduction mode. The currents of phase A and B are measured by two current sensors, respectively. The analog signals are sent first to the A/D converter with 12-bit resolution first, and then to FPGA. A photoelectric encoder with 8192 threads is fixed on the motor shaft, and the output signal is sent to a subdivided circuit. And then the angular position with 17 bits can be given. The back EMF of one electrical angle cycle that is measured in Section II is recorded to the external ROM every 0.5°, and the total points are 720. The current back EMF is calculated by the measured angular position and speed. Because there is no torque sensor on the motor shaft, and also the angular acceleration calculated by angular position differential has large noise, the experimental torque waveforms given in this paper are calculated as (4) by measuring the angular speed and the currents of phase A and B.

TABLE I
Parameters of the Gimbal System

Dc-link Voltage	V	28
Loading Rotating Inertia	kg·m^2	0.085
Moment Coefficient	N·m/A	0.774
Back EMF Cofficient	V/rad/s	0.44
Peak Stalling Current	A	2.3
Peak Stalling Torque	N·m	1.78
Phase Resistance	Ω	5.22
Phase Inductance	mh	0.44
Pole Pairs		8
PWM Switching Frequency	kHz	20

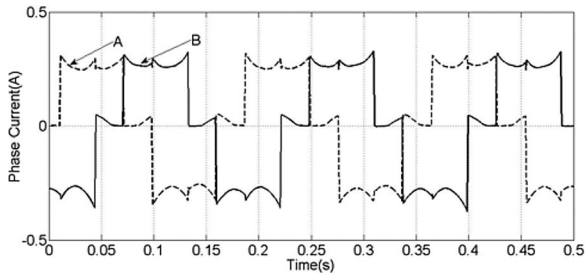

Fig. 15. Measured phase current using H_PWM_L_ON pattern.

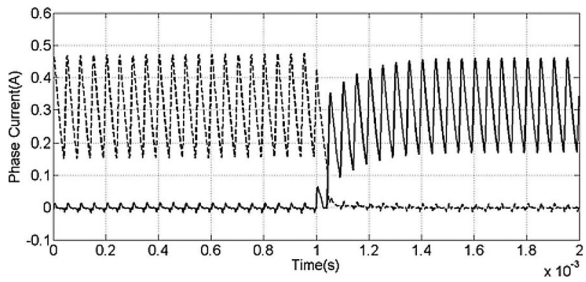

Fig. 16. Measured phase current using H_PWM_L_ON pattern at commutation period.

Figs. 15–17 show experimental waveforms using H_PWM_L_ON pattern on condition that the reference current is 0.3 A and the average angular speed is 4.6 rad/s. Fig. 15 shows the currents of phase A and B, and the diode freewheeling of the inactive phase is obvious. Fig. 16 shows the current waveform of phase A and B at the commutation period. In the commutation period, T1 is switched OFF and T3 is switched ON. The outgoing phase current i_A decreases through the antiparallel diode D1 and the incoming phase current i_B increases through T3. The ripple on the current is produced by the PWM with the carrier cycle of 20 K. It can be seen that the current of phase A can decrease to zero after one PWM period, but it needs six PWM periods for the current of phase B increasing to the steady value. From (5), the conclusion can be drawn that the current ripple occurs on

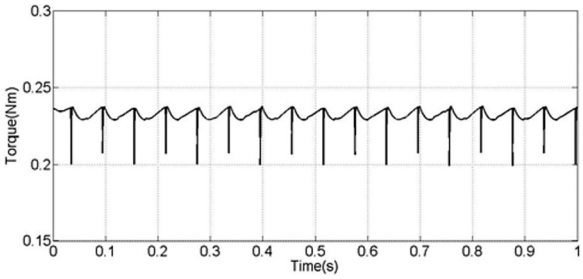

Fig. 17. Measured torque using H_PWM_L_ON pattern.

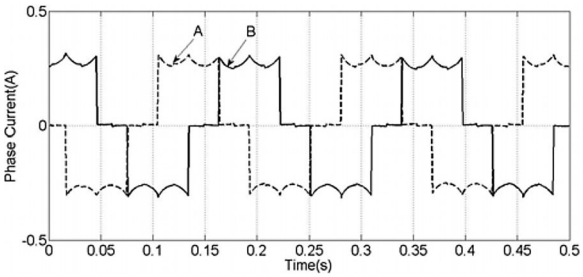

Fig. 18. Measured current of phase A and B using the new current control scheme at low speed.

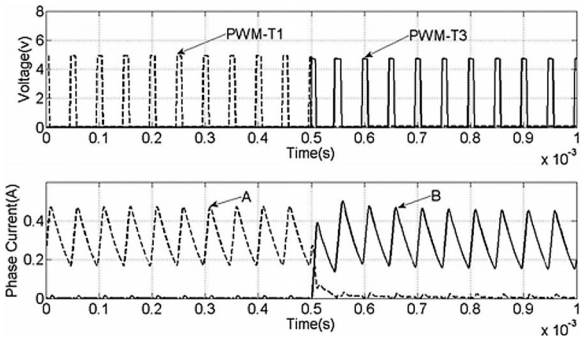

Fig. 19. Measured current and PWM waveform using the new current control method at commutation period at low speed.

the current of phase C and the torque ripple is produced. Fig. 17 shows that the torque ripple is 18% of the output torque using H_PWM_L_ON pattern.

Figs. 18–20 show experimental waveforms using the new current control scheme under the condition that the average angular speed is 4.35 rad/s. From Table I, it can be seen that this condition meets the requirement of $e_A(k) + e_B(k) - 2e_C(k) < u_d$, and the control rule of (34) is used. In Fig. 18, there is no diode freewheeling of inactive phase. In Fig. 19, the duty cycle of switch T3 is increased at the phase-change point when the current outgoing from phase A and incoming to phase B. The current rising rate of phase B current is speed up, which is equal to the current descending rate of phase A's current. In (5), it is shown that there is no current ripple and the torque ripple is eliminated. Fig. 20 shows the calculated torque waveform. It can be seen that the torque ripple is very small and is 4.5% of the output torque when the motor works at low speed.

Figs. 21–23 show experimental waveforms using the new current control scheme under the condition that the average angular speed is 17 rad/s. From Table I, it can be concluded that the working condition meets the requirement of $e_A(k) + e_B(k) - 2e_C(k) > u_d$, so the control rule of (43) is used. Fig. 21 shows the currents of two phases. In this figure there is no diode freewheeling of inactive phase. In Fig. 22, T1 is switched OFF after a little delay time and T3 is switched ON immediately at the phase change point. The current descending rate of phase A is equal to the current rising rate of phase B, and the commutation torque ripple is restrained. Fig. 23 shows the calculated torque waveform. It shows the torque ripple is controlled to 3.4% of the outputting torque.

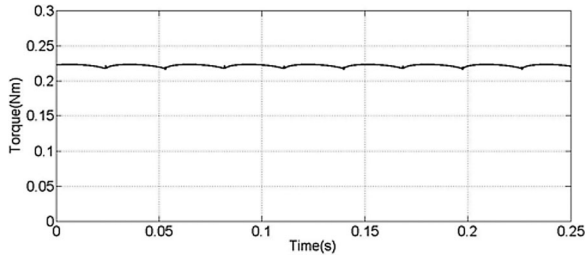

Fig. 20. Measured torque waveform using the new current control method at low speed.

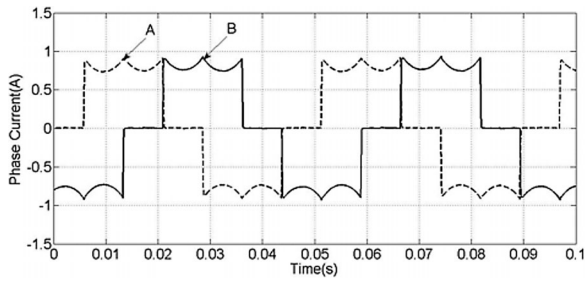

Fig. 21. Measured current of phase A and B using the new current control scheme at high speed.

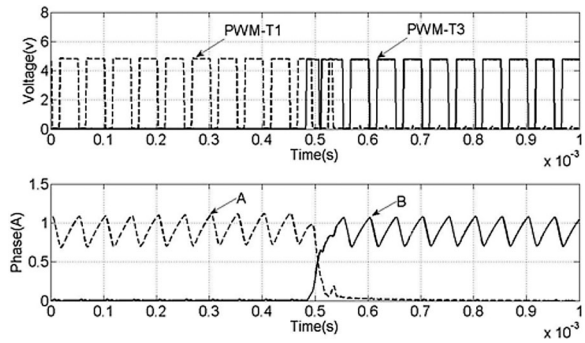

Fig. 22. Measured current and PWM waveform using the new current control method at commutation period with high speed.

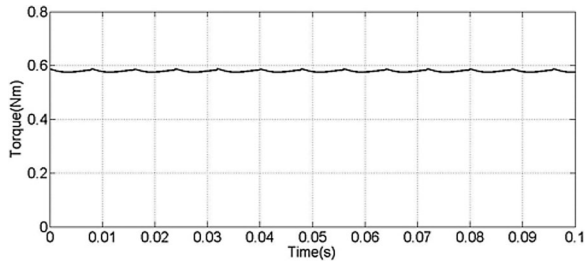

Fig. 23. Measured torque waveform using the new current control method at high speed.

V. Conclusion

In view of the pulsation of three-phase BLDC motor with nonideal back EMF, a new current control method is proposed. The PWM_ON_PWM pattern is used to eliminate the diode freewheeling of inactive phase. When the motor works at low speed, the torque ripple is restrained by speeding up the turn-ON phase current through increasing the duty cycle of PWM. When the motor works at high speed, overlapping commutation scheme is used. The commutation times are given by the current controller in low and high speeds. Aiming at the nonideal back EMF, the duty cycle is calculated in the current controller by measuring the angular position, speed, and the offline measured back EMF. The simulation and experimental results carried out in the gimbal servo system of DGMSCMG validate the validity of the proposed current control method.

References

[1] V. J. Lappas, W. H. Steyn, and C. Underwood, "Design and testing of a control moment gyroscope cluster for small satellites," *J. Spacecraft Rockets*, vol. 42, no. 4, pp. 729–739, 2005.

[2] T. Wei and J. C. Fang, "Dynamics modeling and vibration suppression of high-speed magnetically suspended rotor considering first-order elastic natural vibration," in *Proc. 9th Int. Symp. Magn. Bearings*, 2004.

[3] Z. Wu and J. Y. Zhang, "Dynamics and control of gimbal servo systems for control moment gyroscopes," *J. Basic Sci. Eng.*, vol. 15, no. 1, pp. 130–136, Jul. 2007.

[4] T.-H. Kim and M. Ehsani, "Sensorless control of the BLDC motors from near-zero to high speeds," *IEEE Trans. Power Electron.*, vol. 19, no. 6, pp. 1635–1645, Nov. 2004.

[5] S. B. Ozturk, W. C. Alexander, and H. A. Toliyat, "Direct torque control of four-switch brushless DC motor with non-sinusoidal back EMF," *IEEE Trans. Power Electron.*, vol. 25, no. 2, pp. 263–271, Feb. 2010.

[6] D. Chen and J. C. Fang, "Commutation torque ripple reduction in PM brushless DC motor with nonideal trapezoidal back EMF," in *Proc. CSEE*, Oct. 2008, vol. 28, no. 30, pp. 79–83.

[7] R. Calson, L.-M. Milchel, and J. C. Fagundes, "Analysis of torque ripple due to phase commutation in brushless dc machines," *IEEE Trans. Ind. Appl.*, vol. 28, no. 3, pp. 632–638, May/Jun. 1992.

[8] H. S. Chuang and Y.-L. Ke, "Analysis of commutation torque ripple using different PWM modes in BLDC motors," in *Conf. Rec. IEEE Ind. Commercial Power Syst. Tech. Conf.*, 2009, pp. 1–6.

[9] N. Samoylenko, Q. Han, and J. Jatskevic, "Dynamic performance of brushless DC motors with unbanlanced hall sensors," *IEEE Trans. Energy Convers.*, vol. 23, no. 3, pp. 752–763, Sep. 2008.

[10] J. H. Song and I. Choy, "Commutation torque ripple reduction in brushless DC motor drives using a single DC current sensor," *IEEE Trans. Power Electron.*, vol. 19, no. 2, pp. 312–319, Mar. 2004.

[11] X. F. Zhang and Z. Y. Lu, "A new BLDC motor drives method based on BUCK converter for torque ripple reduction," in *Proc. IEEE Power Electron. Motion Control, Conf.*, 2006, pp. 1–4.

[12] W. Chen, C. L. Xia, and M. Xue, "A torque ripple suppression circuit for brushless DC motors based on power DC/DC converters," in *Proc. IEEE Ind. Electron. Appl. Conf.*, 2006, pp. 1–4.

[13] T. N. Shi, Y. T. Guo, P. Song, and C. L. Xia, "A new approach of minimizing commutation torque ripple for brushless DC motor based on DC-DC converter," *IEEE Trans. Ind. Electron.*, vol. PP, no. 99, pp. 1–9, 2010.

[14] K. Wei, C. S. Hu, and Z. C. Zhang, "A novel commutation torque ripple suppression scheme in BLDCM by sensing the DC current," in *36th IEEE Power Electron. Spec. Conf.*, 2005, pp. 1259–1263.

[15] G.W. Meng, X. Hao, and H. S. Li, "Commutation torque ripple reduction in BLDC motor using PWM_ON_PWM mode," in *Proc. Int. Conf. Electr. Mach. Syst. Conf.*, 2009, pp. 1–6.

[16] K. Seog-Joo and S. Seung-Ki, "Direct torque control of brushless DC motor with nonideal trapezoidal back EMF," *IEEE Trans. Power Electron.*, vol. 10, no. 6, pp. 796–802, Nov. 1995.

[17] G. R. A. Markadeh, S. I. Mousavi, and E. Daryabeigi, "Position sensorless direct torque control of BLDC motor by using modifier," in *Proc. 11th Int. Conf. Optim. Elect. Electron. Equipment*, 2008, pp. 93–99.

[18] J. Gao and Y. Hu, "Direct self-control for BLDC motor drives based on three-dimensional coordinate system," *IEEE Trans. Ind. Electron.*, vol. 57, no. 8, pp. 2836–2844, Aug. 2010.

[19] T. Geyer, G. Papafotiou, and M. Morari, "Model predictive direct torque control—Part I: Concept, algorithm, and analysis," *IEEE Trans. Ind. Electron.*, vol. 56, no. 6, pp. 1894–1905, Jun. 2009.

[20] L. Lianbing, J. Hui, Z. Liqiang, and S. Hexu, "Study on torque ripple attenuation for BLDCM based on vector control method," in *Proc. 2th Int. Conf. Intell. Netw. Intell. Syst.*, 2009, pp. 605–608.

[21] K.-Y. Nam, W.-T. Lee, and C.-M. Lee, "Reducing torque ripple of brushless DC motor by varying input voltage," *IEEE Trans. Magn.*, vol. 42, no. 4, pp. 1307–13210, Apr. 2006.

[22] F. Aghili, M. Buehler, and J. M. Hollerbach, "Optimal commutation laws in the frequency domain for PM synchronous direct-drive motors," *IEEE Trans. Power Electron.*, vol. 15, no. 6, pp. 1056–1064, Nov. 2000.

[23] F. Aghili, "Ripple suppression of BLDC motors with finite driver/amplifer bandwidth at high velocity," *IEEE Trans. Control Syst. Technol.*, vol. PP, no. 99, pp. 1–7, 2010.

[24] H. Lu, L. Zhang, and W. Qu, "A new torque control method for torque ripple minimization of BLDC motors with un-ideal back EMF," *IEEE Trans. Power Electron.*, vol. 23, no. 2, pp. 950–958, Mar. 2008.

Jiancheng Fang was born in September 1965. He received the B.S. degree from the Shandong University of Technology (now Shandong University), Jinan, China, in 1983, the M.S. degree from Xi'an Jiaotong University, Xi'an, China, in 1988, and the Ph.D. degree from Southeast University, Nanjing, China, in 1996.

He is the Dean of the School of Instrumentation Science and Optoelectronics Engineering, Beijing University of Aeronautics and Astronautics, Beijing, China. He has authored or coauthored more than 150 papers and four books. He has been granted 35 Chinese invention patents as the first inventor. His current research interests include focuses on the attitude control system technology of spacecraft, novel inertial instrument and equipment technology, inertial navigation, and integrated navigation technologies of aerial vehicles.

Dr. Fang has the special appointment professorship with the title of "Cheung Kong Scholar," which has been jointly established by the Ministry of Education of China and the Li Ka Shing Foundation. He is in the first group of Principal Scientists of the National Laboratory for Aeronautics and Astronautics of China. He received the first-class National Science and Technology Progress Award of China as the third contributor in 2006, the first-class National Invention Award of China as the first inventor, and the second-class National Science and Technology Progress Award of China as the first contributor in 2007.

Haitao Li was born in 1979 in Shandong, China. He received the B.S. and M.S. degrees from Shandong University, Jinan, China, in 2002 and 2005, respectively, and the Ph.D. degree Beijing University of Aeronautics and Astronautics, Beijing, China, in 2009.

He is currently a Research Member at the Key National Defense Laboratory of Novel Inertial Instrument and Navigation System Technology, School of Instrumentation Science & Optoelectronics Engineering, Beijing University of Aeronautics and Astronautics, China. His main research interests include magnetically suspended control moment gyro and its nonlinear control.

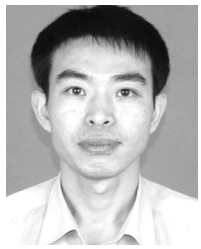

Bangcheng Han was born in February 1974. He received the M.S. degree from Jilin University, Changchun, China, in 2001, and the Ph.D. degree from Changchun Institute of Optics, Fine Mechanics and Physics, Chinese Academy of Sciences, Changchun, China, in 2004.

In 2004, he was a Postdoctoral Research Fellow in the School of Instrumentation Science and Optoelectronics Engineering, Beijing University of Aeronautics and Astronautics, Beijing, China. In 2006, he was with the Beijing University of Aeronautics and Astronautics, where he is currently an Associate Professor in the School of Instrumentation Science and Optoelectronics Engineering. He has more than 20 journal and conference publications. His research interests include mechatronics, magnetic suspension technology, and attitude control actuator of spacecraft.